Self-Assembly of $SrTiO_3$(001) Chemical-Terminations: A Route for Oxide-Nanostructure Fabrication by Selective Growth

R. Bachelet,* F. Sánchez,† J. Santiso,‡ C. Munuera,† C. Ocal,† and J. Fontcuberta†

Institut de Ciència de Materials de Barcelona (ICMAB-CSIC) and Centro de Investigación en Nanociencia y Nanotecnología (CIN2, CSIC-ICN), Campus UAB, Bellaterra 08193, Spain

Received February 23, 2009

We report a method to fabricate functional oxide nanostructures ordered over the centimeter scale. Self-assembly of $SrTiO_3$(001) chemical terminations through appropriate thermal processing leads to large-area chemical nanopattering of the surface. Such nanopatterned surfaces, stable at relatively high temperature, can be used as template to grow functional ordered nanostructures, exploiting the termination-dependent nucleation. As an example of this potential, we have fabricated ordered arrays of conducting epitaxial $SrRuO_3$ nanostripes separated by insulating trenches. Conductivity maps by atomic force microscopy confirm the coexistence of sharp conducting/insulating regions in low-dimensional structures.

1. Introduction

Low-dimensional structures of complex oxides with a wide range of functional properties, from ferroic to catalytic properties, hold the promise to lead to a new generation of materials with unrivalled properties compared to their bulk counterparts. This expectation is at the heart of the unprecedented development of oxide nanostructures. However, nanostructure fabrication of complex oxides is not as well-established as these of metals or semiconductors, which is partly due to the complexity of lattices and the numerous chemical elements. Moreover, the long-range order is even more challenging.

Most oxides are chemically inert to the common etchants, and thus the use of conventional photolithography techniques is very limited.[1] Photolithography by focused ion beam can be used,[2] but it is restricted to pattern only small areas. For larger area production, nanoimprint or electron beam lithographies can be used to create patterns, on which an oxide nanostructure can be fabricated by low-temperature deposition methods.[3−5] Unfortunately, the use of vapor deposition techniques is restricted because high temperatures are usually required. As an alternative, ferroelectric nanostructures were straightforwardly grown through heat-resistant stencil masks as nanoporous anodic aluminum oxide[6−8] or SiN,[9] with deposition temperatures of 650 and 600 °C, respectively. In addition to these top-down approaches, self-organized growth of nanostructures is the alternative cost-effective bottom-up approach to create nanostructures ordered over macroscopic areas.[10] Indeed, self-organized growth of nanostructures has been achieved with different types of materials: organics,[10−12] metals,[13,14] semiconductors,[15] and oxides.[16−23] Achievement of spatial order requires controlling nucleation of nano-objects at specific substrate places. For instance, vicinal substrates[13,14,22] or even corrugated substrates,[21] as well as periodic arrays of dislocations[24,25] have been used for the development of nanodots and/or nanowires arrays. Original oxide nanostructures have been recently developed, as

* Corresponding author. E-mail: rbachelet@icmab.es.
† ICMAB-CSIC.
‡ CIN2, CSIC-ICN.

(1) Martin, C. R.; Aksay, I. A. *J. Electroceram.* **2004**, *12*, 53.
(2) Ganpule, C. S.; Stanishevsky, A.; Su, Q.; Aggarwal, S.; Melngailis, J.; Williams, E.; Ramesh, R. *Appl. Phys. Lett.* **1999**, *75*, 409.
(3) Harnagea, C.; Alexe, M.; Schilling, J.; Choi, J.; Wehrspohn, R. B.; Hesse, D.; Gösele, U. *Appl. Phys. Lett.* **2003**, *83*, 1827.
(4) Pan, Z.; Alem, N.; Sun, T.; Dravid, V. P. *Nano Lett.* **2006**, *6*, 2344.
(5) Clemens, S.; Schneller, T.; van der Hart, A.; Peter, F.; Waser, R. *Adv. Mater.* **2005**, *17*, 1357.
(6) Lee, W.; Ji, R.; Gösele, U.; Nielsch, K. *Nat. Mater.* **2006**, *5*, 741.
(7) Han, C. Y.; Willing, G. A.; Xiao, Z.; Wang, H. H. *Langmuir* **2007**, *23*, 1564.
(8) Lee, W.; Han, H.; Lotnyk, A.; Schubert, M. A.; Senz, S.; Alexe, A.; Hesse, D.; Baik, S.; Gösele, U. *Nat. Nanotechnol.* **2008**, *3*, 402.
(9) Riele, P. M. te.; Rijnders, G.; Blank, D. H. A. *Appl. Phys. Lett.* **2008**, *93*, 233109.
(10) Barth, J. V.; Costantini, G.; Kern, K. *Nature* **2005**, *437*, 671.
(11) Marchenko, O.; Cousty, J. *Phys. Rev. Lett.* **2000**, *84*, 5363.
(12) Barrena, E.; De Oteyza, D. G.; Sellner, S.; Dosch, H.; Oriol Ossó, J.; Struth, B. *Phys. Rev. Lett.* **2006**, *97*, 076102.
(13) Figuera, J.; dela; Huerta-Garnica, M. A.; Prieto, J. E.; Ocal, C.; Miranda, R. *Appl. Phys. Lett.* **1995**, *66*, 1006.
(14) Rousset, S.; Repain, V.; Baudot, G.; Garreau, Y.; Lecoeur, J. *J. Phys.: Condens. Matter* **2003**, *15*, S3363.
(15) Teichert, C. *Phys. Rep.* **2002**, *365*, 335.
(16) Zheng, H.; Wang, J.; Lofland, S. E.; Ma, Z.; Mohaddes-Ardabili, L.; Zhao, T.; Salamanca-Riba, L.; Shinde, S. R.; Ogale, S. B.; Bai, F.; Viehland, D.; Jia, Y.; Schlom, D. G.; Wuttig, M.; Roytburd, A.; Ramesh, R. *Science* **2004**, *303*, 661.
(17) Jiang, J.; Henry, L. L.; Gnanasekar, K. I.; Chen, C.; Meletis, E. I. *Nano Lett.* **2004**, *4*, 741.
(18) Lüders, U.; Sánchez, F.; Fontcuberta, J. *Phys. Rev. B* **2004**, *70*, 045403.
(19) Munuera, C.; Zúñiga-pérez, J.; Rommeluere, J. F.; Sallet, V.; Triboulet, R.; Soria, F.; Muñoz-Sanjosé, V.; Ocal, C. *J. Cryst. Growth* **2004**, *264*, 70.
(20) Zheng, H.; Zhan, Q.; Zavaliche, F.; Sherburne, M.; Straub, F.; Cruz, M. P.; Chen, L.-Q.; Dahmen, U.; Ramesh, R. *Nano Lett.* **2006**, *6*, 1401.
(21) Bachelet, R.; Cottrino, S.; Nahélou, G.; Coudert, V.; Boulle, A.; Soulestin, B.; Rossignol, F.; Guinebretière, R.; Dauger, A. *Nanotechnology* **2007**, *18*, 015301.
(22) Gibert, M.; Puig, T.; Obradors, X.; Benedetti, A.; Sandiumenge, F.; Hühne, R. *Adv. Mater.* **2007**, *19*, 3937.
(23) Park, S.; Horibe, Y.; Asada, T.; Wielunski, L. S.; Lee, N.; Bonanno, P. L.; O'Malley, S. M.; Sirenko, A. A.; Kazimirov, A.; Tanimura, M.; Gustafsson, T.; Cheong, S.-W. *Nano Lett.* **2008**, *8*, 720.
(24) Brune, H.; Giovannini, M.; Bromann, K.; Kern, K. *Nature* **1998**, *394*, 451.
(25) Teichert, C.; Hofer, C.; Lyutovich, K.; Bauer, M.; Kasper, E. *Thin Sol. Films* **2000**, *380*, 25.

10.1021/cm900540z CCC: $40.75
Published on Web 05/07/2009

embedded nanostructures,[20] self-assembled columnar nanorods,[17] or perpendicular self-ordered nanorods,[23] but generally with a lack of long-range ordering or a restriction to particular structures or compositions. Therefore, alternative methods with the capability to produce different long-range ordered nanopatterns are required.

Here, we present an original approach that exploits the presence of two chemical terminations, TiO_2 and SrO, in the widely used $SrTiO_3$(001) surfaces. Taking advantage of the self-organization of chemical terminations and of the termination-dependent nucleation of complex oxides, we show a simple procedure to obtain 1D ordered functional nanostructures.

The cubic perovskite $SrTiO_3$ viewed in the ⟨001⟩ directions is made up from a stack of alternating neutral TiO_2 and SrO layers (spaced out half of one unit cell, i.e., (0.3905/2) nm). It is known that both terminations are randomly present on as-received substrates, and that SrO surface segregation can appear under annealing at high temperature and oxidizing conditions.[26−28] Here, starting from a random distribution of both terminations in as-received surfaces, we will show that by means of appropriate thermal treatments, the SrO termination self-organizes, forming, along the substrate step-edges, a well-ordered array of half-unit-cell-deep trenches coexisting with atomically flat TiO_2 terraces in between. Exploiting differences in adatom sticking coefficient between both atomic terminations, we will demonstrate that this chemically nanopatterned surface can be subsequently used as template to create long-range-ordered 1D nanostructures of functional oxides. To illustrate the potential of this approach, we have grown the metallic (and ferromagnetic) oxide $SrRuO_3$ by pulsed laser deposition on the developed template. We will show that the termination-dependent nucleation of this oxide, without nucleation on SrO trenches, leads to ordered arrays of conducting nanostripes running along the step-edges. These findings demonstrate that the most commonly used $SrTiO_3$ surface can be chemically self-organized and used as a versatile template, opening avenues for large-area production of ordered oxide nanostructures. We note that the concept developed here can be straightforwardly extended to many others functional oxides thanks to differences in sticking coefficients in complex oxides.

2. Experimental Section

The $SrTiO_3$(001) substrates[29] presented here were as-received and thermally treated under air at high temperature (1100 or 1200 °C) for 2 h. All the thermal treatments were realized in a dedicated furnace.

The $SrRuO_3$ films were realized by pulsed laser deposition. A KrF excimer laser ($\lambda = 248$ nm) at a repetition rate of 1 Hz was focused on a rotating stoichiometric $SrRuO_3$ target at a fluence of about 2.5 J cm^{-2}. The target-substrate distance was fixed to 53 mm. During deposition, the sample temperature and oxygen pressure were kept at 700 °C and 13 Pa, respectively. A differentially pumped 30 keV reflection high energy electron diffraction (RHEED) was used to monitor the growth in real time. The specular RHEED intensity was recorded in one-beam conditions (∼10° off-azimuthal $[100]_{SrTiO_3}$ direction), with an incidence angle of ∼1° and a video-camera time resolution of ∼100 ms.

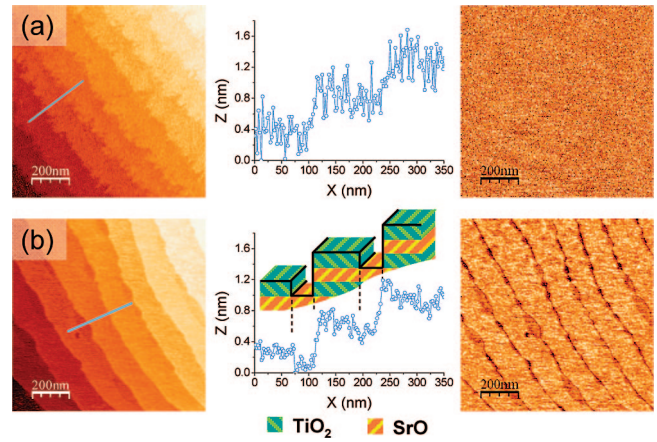

Figure 1. AM-AFM topographic (left panels) and simultaneous phase-contrast (right panels) images of (a) as-received and (b) (1100 °C, 2 h)-air-annealed $SrTiO_3$(001) substrates. Central panels show the corresponding topographic profiles. A sketch of the deduced surface nanostructure has been placed correspondingly above the topographic profile.

Atomic force microscopy working in tapping mode (amplitude modulation AFM) in ambient conditions was used to investigate (i) the surface morphology of the samples and (ii) the spatial distribution of the chemical terminations of the $SrTiO_3$(001) surfaces by phase contrast imaging. To confirm the presence of both chemical terminations as well as their patterned structure, we employed the contact AFM operation mode in low-humidity conditions (2% of relative humidity (RH) in a N_2 flux), next to a short annealing at 400 °C to remove possible adsorbed water, to simultaneously acquire topography and friction force measurements. Rectangular cantilevers using Si_3N_4 tips of ∼10 nm of initial radius (from Scientec and Nanosensors) were employed. Conductive-AFM was used to map the electrical conductivity response of the $SrRuO_3$ nanostructures, with the help of a conducting Si_3N_4 tip coated by boron-doped diamond and applying a bias voltage of $V = 500$ mV. The sample was always grounded and the voltage was applied to the tip. Direct electric sample contact to ground is established through a silver epoxy drop at the film border. This latter experimental setup is sketched in the inset of Figure 5a.

3. Results and Discussion

3.1. Chemical Nanopatterning of $SrTiO_3$(001) Surface. The morphology of $SrTiO_3$(001) surfaces can be observed in the amplitude modulation atomic force microscopy (AM-AFM) images of Figure 1. Left panels are topographic images, right panels are the corresponding phase-contrast images and central panels are the height profiles measured along the indicated lines on the corresponding topographic images. In the topographic image of the as-received substrate[29] (Figure 1a), distinguishable steps and terraces can be observed having very irregular step-edges. The height profile shown in the central panel of Figure 1a reveals the existence of one unit-cell (u.c.) steps to which a fluctuating signal of amplitude larger than the level of noise is superimposed. This likely reflects the coexistence of random distribution of TiO_2 and SrO terminations that coexist in untreated substrates. Because of the limited lateral resolution

(26) Szot, K.; Speier, W. *Phys. Rev. B* **1999**, *60*, 5909.
(27) Huijbregtse, J. M.; Rector, J. H.; Dam, B. *Physica C* **2001**, *351*, 183.
(28) Ohnishi, T.; Shibuya, K.; Lippmaa, M.; Kobayashi, D.; Kumigashira, H.; Oshima, M.; Koinuma, H. *Appl. Phys. Lett.* **2004**, *85*, 272.
(29) From CrysTec GmbH, http://www.crystec.de/crystec-e.html.

of AFM, these different terminations are not discriminated in the corresponding phase image (right panel), which would be otherwise chemically sensitive.[30,31]

The effect of high-temperature annealing on the surface nanostructure of as-received substrates can be appreciated in Figure 1b, where the AFM images taken after thermal treatment under air (2 h, 1100 °C) of the very same crystal are shown. Inspection of the topographic image reveals that high-temperature annealing leads to a great smoothing of the virgin surface (Figure 1a) with formation of smoother step-edges and flatter terraces (rms = 0.18 nm). However, detailed examination shows some darker (lower height) regions aligned along ascending step-edges. Indeed, the corresponding height profile (central panel) shows the existence of low-lying trenches adjacent to step-edges, up to ~40 nm wide and depressed by 1/2 u.c. below the neighboring descending terrace [see sketch in Figure 1b (central panel)]. Because of the alternating composition of 1/2 u.c. stacked layers in $SrTiO_3$(001), the 1/2 u.c. height difference between exposed regions points to a possible difference in their chemical termination. This fact is verified by the corresponding phase lag image (right panel), which clearly shows a strong contrast at the trenches. Provided the phase shift signal in the amplitude modulation AFM operation mode changes with variation in the dissipated energy on different materials, the contrast between surface regions reveals their different nature.[30,31] It thus follows that the chemical composition at the trenches along steps-edges differs from that of flat terraces. As SrO termination is minority under the used processing conditions[28] and steps and neighboring strained regions are known to be favorable sites for SrO nucleation and/or recrystallization,[26] we conclude that the deep trenches lying along step-edges are likely regions formed by coalescence and self-ordering of native SrO termination. The substrate shown in Figure 1 has a miscut angle of 0.14°, but the same annealing effect has been verified with substrates of different miscut angles ranging from 0.06 to 0.16° (see Figure 4 below and the Supporting Information).

To further verify the different chemical nature of flat terraces and trenches, we performed friction force microscopy maps (FFM).[32] To quantify the difference between friction responses, we acquired simultaneous topographic and lateral force (forward and backward) images in low-humidity conditions (2% RH in a N_2 flux). In the topographic image (Figure 2a), and in agreement with results presented in Figure 1b, the incipient formation of trenches along step-edges is well visible, with smooth step-edges and flat terraces separated by 1/2 u.c. deep low-lying regions. The lateral-force (F_L) images shown in Figure 2b evidence a clear friction contrast between the flat terraces and the trenches, confirming differences in chemical-termination, in agreement with the AM-AFM phase-contrast images. The calculated resulting friction force is displayed with the corresponding

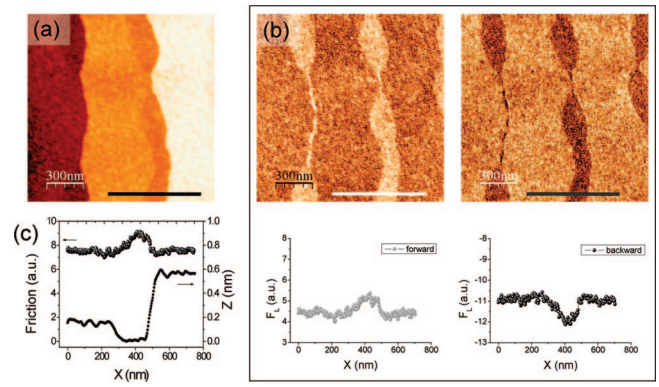

Figure 2. Topographic and friction data simultaneously acquired on 1100 °C-annealed $SrTiO_3$(001) substrate shown in Figure 1b. (a) Topographic image; (b) lateral force images and the corresponding profiles, forward (left) and backward (right); (c) resulting friction force shown with the topographic profile. The trenches (brighter regions in the forward scan) correspond to the higher-friction SrO regions (see text).

height profile in Figure 2c. The friction is quantified to be about 15% higher at the trenches (brighter regions in the forward images) than at the terraces. This percentage reached values close to 35−40% under higher humidity conditions (measurements not shown here), likely due to an enhanced water adsorption on the more hydrophilic SrO termination.[33−36] We thus confirm the nature of the trenches regions as SrO-terminated. The observed self-ordering of SrO (and consequently TiO_2) termination on $SrTiO_3$(001) surfaces implies chemical self-assembly and atomic diffusion. For this process to occur, a driving force must exist promoting SrO enrichment at step edges. On the basis of previous results indicating preferential nucleation of SrO nanocrystals on strained regions of $SrTiO_3$ surface,[26] we suggest that the existing strain field at step-edges may play a similar role.

3.2. Selective Growth of Functional Oxide. We will show hereafter that these nanopatterned surfaces can be used as templates for selective growth of functional oxides. As an example, we have deposited by pulsed laser deposition, the ferromagnetic metallic oxide $SrRuO_3$, which is known to nucleate distinctly on TiO_2 and SrO terminations of $SrTiO_3$(001) surfaces.[37] We have grown two monolayers (ML) of $SrRuO_3$ on the thermally treated substrate presented in Figure 1b. The reflection high energy electron diffraction (RHEED) oscillations shown in Figure 3a indicate layer-by-layer growth. The deposition time (τ) to complete the first ML is greater (×1.5) than that required to complete the second ML, in agreement with previous observations attributing this fact to the volatility of RuO_2 on TiO_2-terminated surface[37] and suggests the growing stacking sequences: SrO-RuO_2−SrO, followed by RuO_2−SrO. The topographic AFM image of the resulting surface is shown in Figure 3b. Clearly, the growth of $SrRuO_3$ proceeds by nucleation on top of the TiO_2-terminated terraces exclusively, leaving uncovered

(30) Magonov, S. N.; Elings, V.; Whangbo, M.-H. *Surf. Sci.* **1997**, *375*, L385.
(31) (a) García, R.; Pérez, R. *Surf. Sci. Rep.* **2002**, *47*, 197. (b) García, R.; Magerle, R.; Pérez, R. *Nat. Mater.* **2007**, *6*, 405.
(32) Carpick, R. W.; Salmeron, M. *Chem. Rev.* **1997**, *97*, 1163.
(33) Fompeyrine, J.; Berger, R.; Lang, H. P.; Perret, J.; Mächler, E.; Gerber, Ch.; Locquet, J.-P. *Appl. Phys. Lett.* **1998**, *72*, 1697.
(34) Iwahori, K.; Watanabe, S.; Kawai, M.; Mizuno, K.; Sasaki, K.; Yoshimoto, M. *J. Appl. Phys.* **2000**, *88*, 7099.
(35) Iwahori, K.; Watanabe, S.; Kawai, M.; Kobayashi, K.; Yamada, H.; Matsushige, K. *J. Appl. Phys.* **2003**, *93*, 3223.
(36) Kato, H. S.; Shiraki, S.; Nantoh, M.; Kawai, M. *Surf. Sci.* **2003**, *544*, L722.
(37) Rijnders, G.; Blank, D. H. A.; Choi, J.; Eom, C.-B. *Appl. Phys. Lett.* **2004**, *84*, 505.

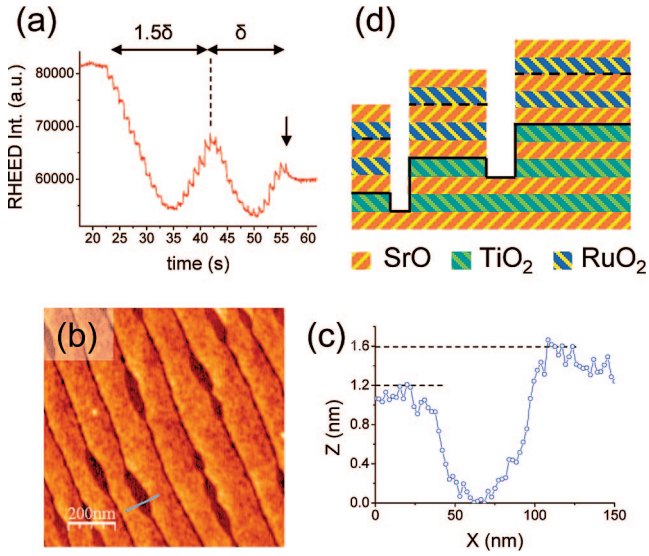

Figure 3. (a) RHEED intensity (specular reflection) acquired during the deposition of the film shown in (b). (b) AFM topographic images of the $SrTiO_3$(001) substrate shown in Figure 1b (annealed in air at 1100 °C for 2 h), after deposition of 2 ML of $SrRuO_3$. Vertical arrow in (a) indicates the time at which film growth was correspondingly stopped. The surface height profile after deposition of 2 ML and the sketch of the corresponding atomic layers are shown in (c) and (d), respectively.

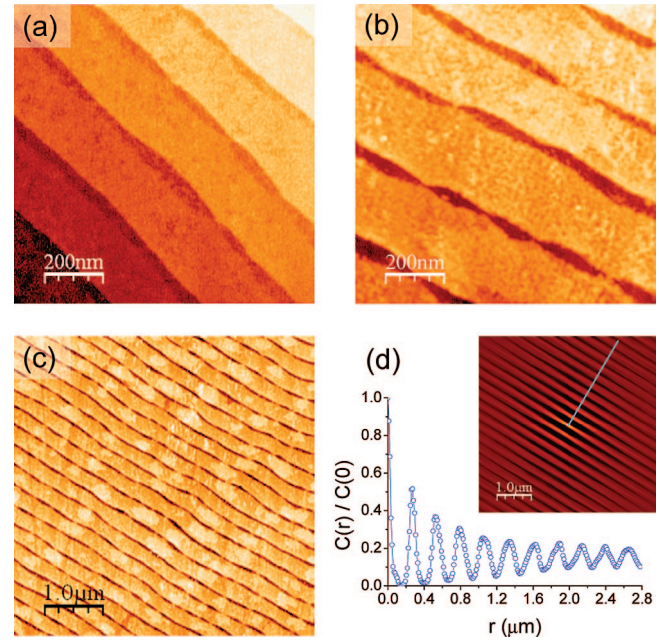

Figure 4. AFM topographic images of: a) bare $SrTiO_3$(001) substrate after annealing at 1200 °C for 2 h. b) 1 × 1 μm^2 and c) 5 × 5 μm^2 areas of a $SrRuO_3$ film (7 ML) deposited on (a). d) Self-correlation function of the image shown in (c) and the corresponding profile taken perpendicular to the steps.

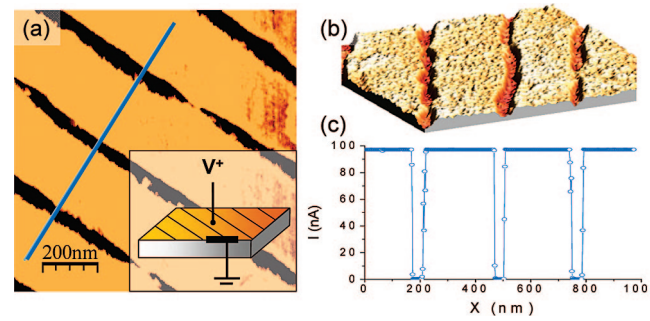

Figure 5. (a) Electrical conductivity map of the $SrRuO_3$ film shown in Figure 4b. Inset: sketch of the measuring setup. (b) 3D topographic view of the nanostructure. To aid visualization, it has been placed above (c) the intensity profile taken along the indicated line in (a). The flat region response in the current profile is due to the saturation of the current amplifier, fixed to 100 nA in the experimental set up used.

the SrO-terminated trenches (dark regions in Figure 3b) of the substrate, where nucleation is unfavorable. The height profile on this surface (Figure 3c) illustrates the presence of deep trenches confined within asymmetric (∼1.2−1.6 nm) walls. We notice that this difference is of about 1 u.c., thus reflecting the initial morphology of the substrate surface with terraces height differing by 1 u.c. The sketch in Figure 3d helps us to understand the profile shown in Figure 3c. The overall altitude of 1.2 nm (and 1.6 nm) is also consistent with the RHEED data and a stacking sequence SrO−RuO_2−SrO−RuO_2−SrO grown on terraces differing by one u.c.

3.3. Fabrication of Conducting Nanostripe Arrays. It is expected that higher temperature annealing under oxidizing conditions should enhance surface diffusion, and eventually promote surface SrO enrichment, improving self-ordering of the template. Thus, in order to increase the trenches homogeneity, an as-received $SrTiO_3$ substrate with a miscut angle of 0.10° was annealed at a still higher temperature (1200 °C for 2 h). The enhancement of the long-range order and homogeneity of the SrO-terminated regions running along step-edges can be appreciated in Figure 4a.

After coverage of 7 ML of $SrRuO_3$ (∼3 nm), the resulting film morphology (Figure 4b) clearly mimics that of the substrate pattern, which acts as template for replication. The quality of the long-range ordering of $SrRuO_3$ and SrO stripes can be better appreciated in the 5 × 5 μm^2 image of Figure 4c and the corresponding self-correlation function (Figure 4d). The persistence of the oscillations in the profile taken perpendicular to the steps (Figure 4d) attests the long-range order. The pattern periodicity of 265 nm (given by the position of the first maximum in the profile) is related to the substrate terrace width, driven by the substrate miscut-angle. We then note that the spacing between trenches, and thus the relative width of $SrRuO_3$ and SrO stripes, can be easily tailored by an appropriate choice of the substrate miscut-angle. We also note that as the film thickness is increased, the separation between SRO stripes progressively diminishes and an atomically flat surface with 1 u.c. high steps arises (see Figure S2 in the Supporting Information).

So far, we have assigned the deep trenches to uncovered SrO substrate regions and consequently they should exhibit an insulating character. To confirm this fact, we have performed current sensing AFM measurements using a conducting tip (C-AFM) on the film surface shown in images b and c in Figure 4. In Figure 5a, we show the map of current flowing between the tip and the sample, recorded by using the experimental setup sketched in the inset of Figure 5a when biasing at V = 500 mV. The insulating nature of the self-ordered trenches sharply

contrasts with the conducting nature of the $SrRuO_3$ stripes covering the terraces. This is emphasized by the intensity line-scan shown in Figure 5c.

The templates developed here could be used to grow other functional nanostructured oxides, such as dielectric interdigitated capacitors or 1D ferroelectric elements but are of interest by themselves for their potential selective catalytic activity. Indeed, $SrTiO_3$[38] and other perovskites such as $BaTiO_3$[39] have caught interest for its photocatalytic properties, which depend on the composition of the atomic termination layer. Moreover, these templates could allow exploitation of spatial separation of charge carriers and reaction products; with an obvious impact on the efficiency of photochemically active ceramics or even for obtaining selective photochemical oxidation/reduction at specific regions of treated $SrTiO_3$ substrates.[40]

4. Conclusions

In summary, we have shown a simple high-temperature annealing process, by which SrO terminations on $SrTiO_3(001)$ surface spontaneously form ordered nanotrenches along step-edges separated by atomically flat terraces in between. Exploiting the difference in adatom sticking coefficients between both chemical terminations, we have further proven that the chemically self-patterned $SrTiO_3(001)$ surfaces can be used as template for fabrication of oxide nanostructures by selective nucleation and growth. This method has allowed us to obtain ordered arrays of conducting $SrRuO_3$ nanostripes separated by insulating trenches. The obtained nanostructures are promising for selective growth of other materials, leading to more complex structures and offering opportunities in the fabrication of functional low-dimension structures.

Acknowledgment. Financial support from the Ministerio de Ciencia e Innovación of the Spanish Government Projects MAT2007-62732, MAT2008-06761-C03, MAT2008-62732, and NANOSELECT CSD2007-00041; from the European Union [Project MaCoMuFi (FP6-03321) and FEDER]; and from ICN is acknowledged. The authors are also grateful to F. Valle, M. Romeu, J. Roqueta, L. Garzón, M. Paradinas, M. Simon, and A. Pérez del Pino for experimental support.

Supporting Information Available: Self-assembly of chemical terminations in $SrTiO_3(001)$ substrates with different miscut angles; evolution of $SrRuO_3$ morphology with thickness: from stripes to continuous film (PDF). This material is available free of charge via the Internet at http://pubs.acs.org.

CM900540Z

(38) Giocondi, J. L.; Rohrer, G. S. *J. Am. Ceram. Soc.* **2003**, *86*, 1182.
(39) Giocondi, J. L.; Rohrer, G. S. *J. Phys. Chem. B* **2001**, *105*, 8275. Giocondi, J. L.; Rohrer, G. S. *Chem. Mater.* **2001**, *13*, 241.
(40) Vasco, E.; Karthäuser, S.; Dittmann, R.; He, J.-Q.; Jia, C.-L.; Szot, K.; Waser, R. *Adv. Mater.* **2005**, *17*, 281.